International Journal of Pharmaceutics 660 (2024) 124340

Contents lists available at ScienceDirect

International Journal of Pharmaceutics

journal homepage: www.elsevier.com/locate/ijpharm

Camptothecin-loaded mesoporous silica nanoparticles functionalized with CpG oligodeoxynucleotide as a new approach for skin cancer treatment

Munibah Qureshi [a], Cláudia Viegas [b,c,d,e], Sofia O.D. Duarte [d,e], Michael Girardi [f], Adeeb Shehzad [a,*], Pedro Fonte [c,d,e,g,*]

[a] Department of Biomedical Engineering and Sciences, SMME, NUST, Islamabad, Pakistan
[b] Faculty of Medicine and Biomedical Sciences (FMCB), Universidade do Algarve, Faro, Portugal
[c] Centre of Marine Sciences (CCMAR), Campus de Gambelas, Universidade do Algarve, 8005-139 Faro, Portugal
[d] iBB—Institute for Bioengineering and Biosciences, Instituto Superior Técnico, University of Lisbon, 1049-001 Lisboa, Portugal
[e] Associate Laboratory i4HB—Institute for Health and Bioeconomy, Instituto Superior Técnico, University of Lisbon, 1049-001 Lisboa, Portugal
[f] Department of Dermatology, School of Medicine, Yale University, New Haven, CT 06520, USA
[g] Department of Chemistry and Pharmacy, Faculty of Sciences and Technology, Universidade do Algarve, Gambelas Campus, 8005-139 Faro, Portugal

ARTICLE INFO

Keywords:
Nanocarrier
Silica nanoparticle
Camptothecin
CpG oligonucleotide
Cutaneous squamous cell carcinoma
Functionalization

ABSTRACT

The therapeutic efficacy of camptothecin (CPT), a potent antitumor alkaloid, is hindered by its hydrophobic nature and instability, limiting its clinical use in treating cutaneous squamous cell carcinoma (SCC). This study introduces a novel nano drug delivery system (NDDS) utilizing functionalized mesoporous silica nanoparticles (FMSNs) for efficient CPT delivery. The FMSNs were loaded with CPT and subsequently coated with chitosan (CS) for enhanced stability and bioadhesion. Importantly, CpG oligodeoxynucleotide (CpG ODN) was attached onto the CS-coated FMSNs to leverage the immunostimulatory properties of CpG ODN, augmenting the chemotherapy's efficacy. The final formulation FMSN-CPT-CS-CpG displayed an average size of 241 nm and PDI of 0.316 with an encapsulation efficiency of 95 %. Comprehensive *in vitro* and *in vivo* analyses, including B16F10 cells and DMBA/TPA-induced SCC murine model, demonstrated that the FMSN-CPT-CS-CpG formulation significantly enhanced cytotoxicity against B16F10 cells and induced complete regression in 40 % of the *in vivo* subjects, surpassing the efficacy of standard CPT and FMSN-CPT treatments. This study highlights the potential of combining chemotherapeutic and immunotherapeutic agents in an NDDS for targeted, efficient skin cancer treatment.

1. Introduction

Epidermal keratinocyte-derived carcinomas, particularly cutaneous squamous cell carcinoma (SCC), are the most prevalent malignancies worldwide (Dessinioti et al., 2021). Several factors, including UV-induced damage from the sun or artificial sources, chronic inflammation and immunosuppression, contribute to the development and progression of SCC (Fania et al., 2021). Surgical resection is the first-line therapeutic approach for localized SCC, whereas systemic treatment is reserved for metastatic SCC. However, these approaches may be limited by risks of recurrence, resistance, and undesirable aesthetic outcomes. Chemotherapy results in serious side effects due to frequent dosing, lack of specificity and selectivity, and poor availability of active components at the tumor site (Yan et al., 2020). Topical treatments such as 5-fluorouracil and imiquimod are only affective for superficial SCCs (Voiculescu et al., 2019). Epidermal growth factor receptor (EGFR) inhibitors offer a new nonsurgical option for advanced SCC but often result in skin side effects, for instance, papulopustular eruptions, pruritus, paronychia and xerosis (Cho et al., 2016). Furthermore, the overall costs of the management and treatment of SCC represent a major economic burden on individuals and national healthcare systems (Gordon and Rowell, 2015), emphasizing the need for the exploration and implementation of more efficient alternatives to alleviate this healthcare challenge.

Camptothecin (CPT) is an indole alkaloid that acts as a DNA topoisomerase I inhibitor (Rev et al., 2008) with broad activity as an anticancer drug in preclinical models. CPT functionality is hampered by its

* Corresponding authors at: Department of Biomedical Engineering and Sciences, SMME, NUST, Islamabad, Pakistan (A. Shehzad); Centre of Marine Sciences (CCMAR), Campus de Gambelas, Universidade do Algarve, 8005-139 Faro, Portugal (P. Fonte).
E-mail addresses: adeeb.shehzad@smme.nust.edu.pk (A. Shehzad), prfonte@ualg.pt (P. Fonte).

https://doi.org/10.1016/j.ijpharm.2024.124340
Received 20 March 2024; Received in revised form 22 May 2024; Accepted 12 June 2024
Available online 13 June 2024

hydrophobicity, poor biostability, rapid physiological inactivation, high risk of systemic toxicity, and multidrug resistance (Li et al., 2006). The development of nano-drug delivery systems (NDDSs) has shown the potential to improve the safety and efficacy of treatment by controlling the rate and timing of drug release at specific locations (Castro et al., 2017; Oliveira et al., 2018; Viegas et al., 2022). Nanocarrier systems, including liposomes, amphiphilic copolymers, dendrimers, hydrogels, micelles, metal nanoparticles (NPs), and mesoporous silica nanoparticles (MSNs) have been developed to deliver several hydrophobic drugs (Fan et al., 2023; Shehzad et al., 2018; Wang et al., 2019). Among these, MSNs are actively investigated for developing next-generation inorganic materials for biomedical applications (Zhou et al., 2018), particularly in the field of drug delivery systems, owing to their unique mesostructured properties such as large surface area, large pore volume, modifiable particle size, easy surface functionalization, outstanding biocompatibility, and unique surface-decorating properties with targeting moieties due to the presence of abundant silanol groups (Si-OH) (Cordeiro et al., 2022; Koohi Moftakhari Esfahani et al., 2022). Water molecules can degrade mesoporous silica by hydrolyzing and dissolving the silica framework (Hu et al., 2021a). However, the degradation of MSN can be reduced using a higher pH, lower temperature, and coating of the silica framework (Choi and Kim, 2019). Tailoring the pore characteristics and surface properties of MSNs with other molecules, including organic and inorganic entities, drug molecules, and biological membranes, offers a promising approach for the development of formulations, capable of efficient drug loading and release of hydrophobic drugs into tumors (Koohi Moftakhari Esfahani et al., 2022).

Among various polymeric materials, chitosan (CS) is a natural polysaccharide derived from chitin found in the exoskeletons of crustaceans and the cell walls of fungi (Jafernik et al., 2023). CS has been widely used as a protective shell around the core owing to its biocompatibility, biodegradability, nontoxicity, solubility, bioadhesiveness/mucoadhessiveness, and pH-sensitive properties (Shakeran et al., 2021; Sharifi-Rad et al., 2021). Its application in DDS has been extensively explored for its ability to modulate drug release profiles, enhance cellular uptake, and protect encapsulated drugs from degradation (Sharifi-Rad et al., 2021). It forms electrostatic interactions with negatively charged molecules on biological surfaces through its carboxyl and amino groups (Viswanadh and Muthu, 2018). Various strategies have been proposed to prolong the drug residence time by enhancing contact with the cell surface, thus improving the therapeutic efficacy of local drug delivery (Yu et al., 2022).

Combination approaches in NDDS are promising for the treatment of cancer that can simultaneously transport and deliver different types of therapeutic molecules, such as drugs, immunomodulatory agents, or genetic material (Han et al., 2019; Viswanadh and Muthu, 2018). Furthermore, various ligands, including single- and double-stranded nucleic acid aptamers, have been employed to improve the accumulation of drug-loaded NPs at tumor sites and to reduce off-target side effects (Andrade et al., 2015; Cordeiro et al., 2022; Viegas et al., 2023). These oligonucleotide strands, characterized by their specific 3D folding, engage with distinct cell surface markers, facilitating the selective transportation of tagged NPs to tumor tissues (Babaei et al., 2020b). CpG oligonucleotides (CpG ODN) are synthetic, single-stranded DNA molecules comprising unmethylated cytosine-phosphate guanine motifs, with specific sequences resembling bacterial DNA. The immune system recognizes these sequences through toll-like receptor 9 (TLR9), expressed in certain immune cells, and activates antigen-presenting cells (APCs), such as dendritic cells (DCs), B cells, and macrophages (Tao et al., 2015). Preclinical and clinical studies have confirmed the potential of CpG ODNs as immune adjuvants in cancer immunotherapy (Chehelgerdi et al., 2023; Ezoe et al., 2020; Fehér, 2019; Honda-Okubo et al., 2023; Hu et al., 2021b; Otsuka et al., 2022). The use of MSN as carriers with or without surface modification has been reported to successfully deliver various anticancer drugs, including methotrexate (Shakeran et al., 2021), doxorubicin (Amin et al., 2022; Carrera Espinoza et al., 2021), paclitaxel (Gao et al., 2019), gemcitabine (Saini and Bandyopadhyaya, 2020; Zaharudin et al., 2020), curcumin (De Oliveira et al., 2017), and CPT (Jackson et al., 2023; Min et al., 2023). The acidic pH of the tumor microenvironment has become the main focus of various studies because of its difference from the normal extracellular physiological pH, which leads to the development of pH-responsive NDDS. Numerous molecules and polymers have been used to modify MSN to formulate pH-sensitive and bioadhesive NPs, including folic acid (Gomes et al., 2022), poly acrylic acid (Kundu et al., 2020; Saroj and Rajput, 2018), polyethylenimine (PEI) (Choi and Kim, 2019; Sun et al., 2019), transferrin [42,45], polylactic acid-—hyperbranched polyglycerol (PLA-HPG) (J.K. Hu et al., 2021; Yu et al., 2022), and alginate (Abasalizadeh et al., 2020).

In this study, we developed a nanoplatform for CPT delivery by encapsulating CPT within MSN and then coating it with CS to enhance biocompatibility, control, and prevent drug release to off-target sites due to difference in the pH of healthy and diseased cells. Finally, the system was functionalized with CpG ODNs to enable targeted delivery and immunostimulation, to maximize the therapeutic efficacy. This strategy was evaluated *in vitro* using B16F10 melanoma cells and *in vivo* in a murine skin carcinoma model using local drug delivery via intratumoral injection. The formulated NDDS demonstrated good biocompatibility and high anti-tumor cytotoxic effects both *in vitro* and *in vivo*, particularly when delivered synergistically as a ligand-targeting strategy.

2. Materials and methods

For the NPs formulation, tetraethyl orthosilicate (TEOS, 98 %), (3-aminopropyl) triethoxysilane (APTES, ≥98 %), cetyltrimethylammonium bromide (CTAB, 25 wt%), ammonium hydroxide, glutaraldehyde (GA) solution (25 wt%) and, (S)-(+)-Camptothecin (CPT ≥ 90 %), ethidium bromide (EB), phosphate buffered saline (PBS) were purchased from Sigma-Aldrich (St. Louis, MO, USA.). Ethanol (EtOH, HPLC grade), dimethyl sulfoxide (DMSO), hydrochloric acid (HCl, ACS reagent, fuming, 37 %), chitosan (CS), and glacial acetic acid (<99 %) were obtained from Merck Millipore (Billerica, MA, USA). CpG ODN 1826 (type B,TLR9 ligand) was purchased from InvivoGen (CA, USA). All reagents and solvents used were of analytical grade. Deionized (DI) water was used in all experiments.

For *in vitro* and *in vivo* studies, the murine melanoma cell line B16F10 was provided by the Korean Cell Line Bank (KCLB) (Seoul, Korea). 3-(4,5-dimethylthiazol-2-yl)-2,5diphenyltetrazoliumbromide (MTT), 7,12-dimethylbenz[a]-anthracene (DMBA)) (≥95 % pure), and 12-O-tetradecanoylphorbol-13-acetate (TPA) (≥98 % pure) were obtained from Sigma-Aldrich (St. Louis, MO, USA). Antibiotics (penicillin–streptomycin) were from Gibco, USA, DMEM medium, and fetal bovine serum from Thermo Fisher Scientific. 4 to 6-week-old male BALB/c mice were purchased from the National Institutes of Health (NIH), Islamabad, Pakistan.

2.1. Synthesis of functionalized MSNs

MSNs were formulated using a modified version of the previously reported Stöber method, a type of sol-gel process (Babaei et al., 2020). Briefly, 250 mg of CTAB was dissolved in 120 mL of DI water, followed by the addition of 1 mL of 2 M NaOH. This solution was then heated to 80 °C. Upon reaching this temperature, 1.08 mL TEOS and 110 μL of APTES were added in a molar ratio of 10:1. This mixture was sonicated, stirred, and maintained at 80 °C overnight to form a gel. Subsequently, the particles were washed repeatedly at 6000 rpm for 25 mins, 3 times with ethanol and 3 times with DI water to remove the surfactant, until the supernatant appeared clear and free of foam. The NPs were redispersed in DI water and dried under a vacuum. The functionalized MSNs are referred to as FMSN, while the non-functionalized ones, as MSNs.

2.2. Drug loading

MSNs and FMSNs, each weighing 45 mg, were dispersed in 1 mL of a CPT solution (2.5 mg/mL) in DMSO. To disperse the mixture, it was first sonicated on ice for 5 mins and then stirred at a cold temperature while protecting it from light. The resulting suspension was collected at three different time points (6 h, 12 h, and 24 h), centrifuged at 10,000 rpm for 20 mins at 4 °C, and this process was repeated 4 times with DI water. The NPs were then resuspended in a specific volume of DI water, and lyophilized. The drug-incorporated NPs are referred to as MSN-CPT and FMSN-CPT.

2.3. Chitosan coating of NPs and crosslinking by glutaraldehyde (GA)

FMSNs or FMSN-CPT were dispersed in DMSO. 1 % (v/v) GA was added to the reaction mixture, dropwise and allowed to react for 1 h followed by the addition of 1 % (w/v) CS (4 mL) in 1 % (v/v) acetic acid. After sonication, the mixture was stirred for 8–10 h. The blank NPs were coated with CS using the same method. The resulting suspensions were then washed by centrifugation at 10,000 rpm at 4 °C for 20 mins, four times with DI water, resuspended in a certain amount of DI water, and lyophilized. The NPs were denoted as FMSN-GA-CS and FMSN-CPT-GA-CS.

2.4. Tagging of NDDS with CpG ODN

CpG ODN (5′-tccatgacgttcctgacgtt-3′), a TLR9 agonist of the B Type, was diluted in ultrapure endotoxin-free water to a concentration of 1 mg/mL. The solution was stored in aliquots at −20 °C. The formulated FMSN-CPT-GA-CS NPs were then functionalized with CpG ODN. After the coating process, the suspension was centrifuged to remove any unbound GA and CS. CpG ODN at a concentration of 1 μg/μL in sterile, endotoxin-free water was then added to the reaction, kept at ambient temperature, and gently shaken for 2 h. The resulting suspension was centrifuged at 10,000 rpm for 20 mins at 4 °C, repeated 4 times with DI water. Subsequently, the NPs were resuspended in DI water to achieve a specific concentration and stored at −20 °C until further use. CpG ODN concentration was determined using a Nanodrop Spectrophotometer (NanoDrop 2000, Thermo Scientific), a UV-spectrophotometer, and through gel electrophoresis. Both free CpG ODN and NPs were loaded onto 3 % agarose gels containing EB. The gels were run with a loading buffer at 120 V for 20 mins.

2.5. CPT quantification

The amount of CPT loaded into the carrier was quantified by a UV–Vis spectrophotometer (λmax = 366 nm). CPT entrapment efficiency (EE %) and drug-loading capacity (DLC %) were calculated as follows:

EE % = [mass of loaded drug in a carrier/total amount of drug initially used] × 100.

DLC % = (mass of CPT in carrier)/ (total mass of carrier) × 100.

2.6. Characterization of NPs

The size distribution and surface morphology of the NPs were investigated using a Scanning Electron Microscope (SEM) equipped with an energy-dispersive X-ray microanalysis system (EDX) (JSM-6490A, JEOL, Tokyo, Japan). The hydrodynamic size, polydispersity index (PDI) and zeta potential of the NPs were determined using Dynamic Light Scattering (DLS) and electrophoretic light scattering (ELS) (Zetasizer Nano ZS90 DLS system, Malvern Instruments Ltd., England). Brunauer-Emmett-Teller (BET) analysis (Gemini VII 2390 V1.03) was used for surface characterization, including pore characteristics. To evaluate the thermal behavior (Δw %) and extent of surface modification of MSNs, thermogravimetric analysis (TGA) (TGA/SDTA851e, Schwerzenbaclz, Switzerland) was carried out at a heating rate of 10 °C. min^{-1} up to 700 °C. Further, the chemical interactions between CS, CPT, and carrier were studied using Fourier-Transform Infrared Spectroscopy (FTIR) (Bruker Platinum ATR model Alpha, Ettlingen, Germany) by analyzing a sample in the range of 4000 cm^{-1} to 450 cm^{-1} with an average of 16 scans per sample. The CPT loading within the NPs was quantified using ultraviolet–visible spectroscopy analysis (UV − 3600i Plus UV − Vis-NIR spectrophotometer, Shimadzu Co., Kyoto, Japan).

2.7. In vitro release assay

To evaluate the rate of drug release from all groups of NPs, a known volume of CPT (100 μL) with known concentration was loaded into a Slide-A-Lyzer Mini dialysis units 10 KDa MWCO (ThermoFisher) in triplicate. These units were then incubated at 37 °C. The drug was allowed to be released in 1 mL of 1X PBS at pH 7.4 and pH 6.4, with gentle shaking to facilitate the process. The released medium was collected and replaced with fresh 1x PBS at specific intervals. The CPT concentration in the dialyzed fluid was quantified using a Multiskan Sky microplate reader (Thermo Fisher Scientific).

2.8. In vitro cytotoxicity assay

The cytotoxicity of NDDS was assessed using the MTT assay as previously described (Min et al., 2023). The murine melanoma cell line B16F10 was cultured in 96-well plates (5,000 cells per well) in DMEM medium containing 1 % (v/v) antibiotic (penicillin–streptomycin) and 5 % heat-inactivated fetal bovine serum at 37 °C, in a 5 % CO_2-humidified atmosphere. The cells were washed with PBS after 24 h and treated with various concentrations of FMSN, free CPT, FMSN-CPT, FMSN-CPT-GA-CS and FMSN-CPT-GA-CS-CpG for 24 h, 48 h, and 72 h, and analyzed with MTT reagent (2 mg/mL) solution by spectrophotometry (570 nm).

2.9. Anticancer potential of NDDS against the carcinogenic model

A preclinical cutaneous chemical carcinogenesis model was established, based on a previously reported protocol with slight modifications made for experimental refinement (Vähätupa et al., 2019). This protocol was approved by the Research Ethics Committee of the National University of Sciences and Technology (NUST) (IRB No. 04–2021-02/36), in accordance with the National Institutes of Health Guide for the Care and Use of Laboratory Animals (Bayne, 2011). Male BALB/c mice, 4 to 6 weeks old, and averaging 20 g in weight, were acclimatized for 1 week. The dorsal skin of these mice was shaved (approximately 3 × 3 cm) using electric clippers.

Before starting the experiment, a preliminary study was conducted to determine the dose and frequency of carcinogens and drugs required to induce and treat skin cancers. A single dose of DMBA (200 nmol) was applied to the shaved dorsal skin of mice to initiate tumorigenesis. Starting one week after initiation, TPA (8 nmol) was applied twice a week (up to 10 weeks) to promote tumor progression. The mice were monitored daily and weighed weekly. Only tumors with a diameter of more than 2 mm that remained for not less than one week were classified as papillomas and were recorded. The volume of tumors was calculated using the formula: $1/2 \times (\text{length} \times \text{width}^2)$.

Following the establishment of papillomas, animals were randomized into five distinct groups (n = 7): PBS, free CPT, FMSN-CPT, FMSN-CPT-GA-CS, and FMSN-CPT-GA-CS-CpG. The PBS group served as a positive control. The free CPT group received intratumoral injections twice a month, with a 15-day interval between the administrations. The remaining groups followed the same treatment schedule. The experimental plan is illustrated in Fig. 6A. The animals were euthanized at the end of the study, and skin samples were excised and collected for histological evaluation.

2.10. Statistical analysis

All data were acquired in triplicate and expressed as mean ± standard error of the mean (SEM). The results were statistically analyzed using Origin pro2023b and GraphPad Prism 8 with a *t*-test or one-way ANOVA as applicable. Post Hoc, Tukey's Multiple Comparison Analysis was employed for multiple comparisons, with the significance level set at $p \leq 0.05$.

3. Results and discussion

3.1. Synthesis, modification and characterization of MSNs

A schematic representation of the NPs formulation process is shown in Fig. 1. MSNs were synthesized according to the Stöber method (sol–gel), with some modifications (Gustavson and Miyake, 2016; Werner stober, 1968). Hydrolysis and condensation reactions were performed using TEOS as the silica precursor and CTAB as the template. The modification of hydroxylated MSNs (MSN-OH) with APTES created a siloxane network with positively charged NH_2 head groups that can electrostatically bind to negatively charged molecules, such as DNA, RNA, proteins, drugs, anionic dyes, and polysaccharides. This allowed the successful incorporation of the negatively charged CPT through hydrophobic interactions. CS was then coated onto the drug-incorporated FMSNs using GA as a crosslinker. GA is a commonly used crosslinking agent that reacts with primary amines to form an imine (N = C) bond between the primary amines and aldehyde carbon to form a stable coating. When the CS coating was carried out without GA, only a minor change was observed in the weight of the end product after washing and drying the NPs. This might be due to the lightly bound CS layer, whereas the use of GA resulted in a more stable and firmly bound layer on the surface of the FMSNs, which was also supported by previous studies (Shakeran et al., 2021). The yield of MSNs obtained was 454 mg ± 23 mg, but it varies typically with reaction conditions and particularly the method of drying. The percentage of CS coated on the FMSNs was evaluated by recording the weight of the FMSNs before and after coating (initial and final weights) to determine the weight gain of the end product (ΔW% = (Wf − Wi/Wi) × 100). The weight gain, ΔW = 45 % was calculated after coating FMSNs with 1 % CS. The last step in the fabrication process was the binding of CpG ODN to FMSN-CPT-CS to stimulate and enhance the therapeutic action. The successful fabrication of NPs was characterized and confirmed at each step, starting from the synthesis of bare MSNs to the binding of CpG ODN, ensuring the accessibility and controllable release of the encapsulated drug

3.2. Dynamic light scattering (DLS) and electrophoretic light scattering (ELS)

The hydrodynamic size and PDI for the particle size distribution, and zeta potential were measured using DLS and ELS, respectively. MSN-OH particles showed an estimated average hydrodynamic size of 195 nm with a zeta potential of − 23.7 mV (Fig. 2E, 2F) because of the presence of siloxane groups (−Si-O-), derived from the deprotonation of silanol groups (Si-OH) (Cheng et al., 2020). Modification of MSN-OH to FMSN slightly increased the size but shifted the zeta potential to + 35.5 mV (Fig. 2F) because of the protonation of the NH_2 group. Loading of the drug into the FMSN increased the overall size of the NPs to approximately 244 nm and decreased the zeta potential to + 21 mV because of the negatively charged CPT (Fig. 2F). The coating of FMSN NPs with a positively charged polymer, CS, further modified their size to 269 nm and increased their charge to + 43.6 mV. Binding CpG to CS-coated FMSN caused a further increase in size to 291 nm and reduced the charge to + 29.8 mV (Fig. 2F). CpG ODN typically carries a negative charge due to its phosphate backbone, while CS is a cationic polymer

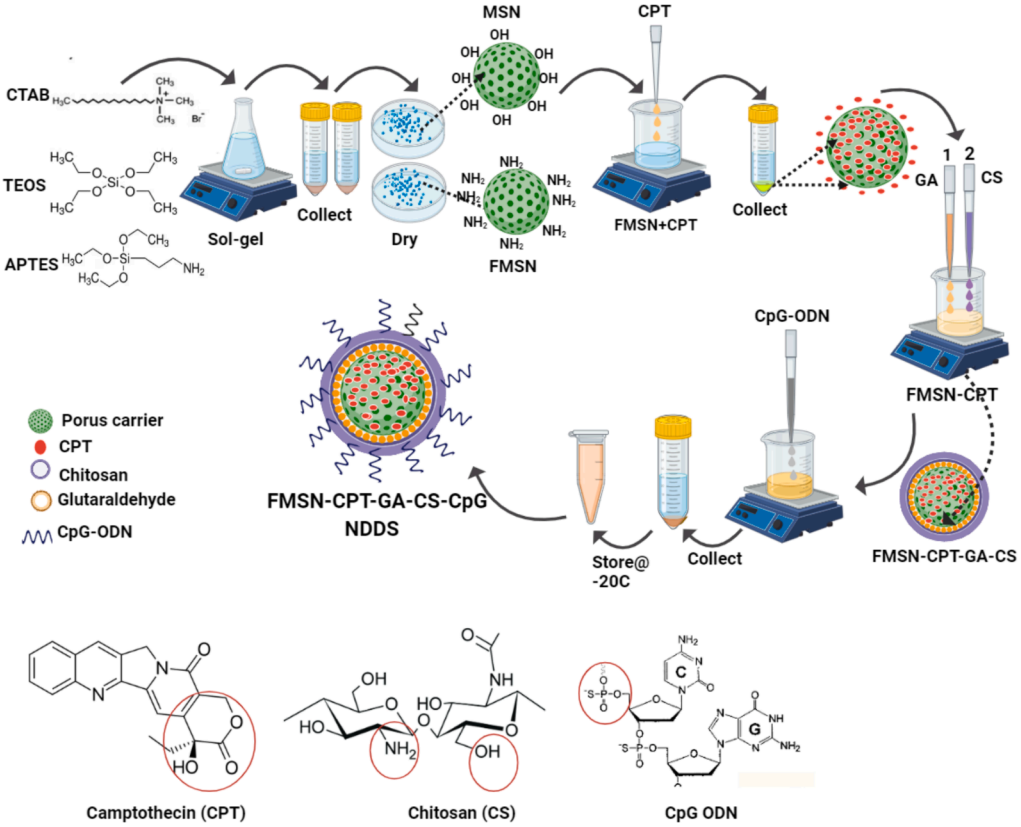

Fig. 1. Schematic representation of NDDS formulation, beginning with the synthesis of MSN to FMSN-CPT-GA-CS-CpG. The chemical structures of CPT, CS, and CpG ODN with encircled active groups, involved in the interaction.

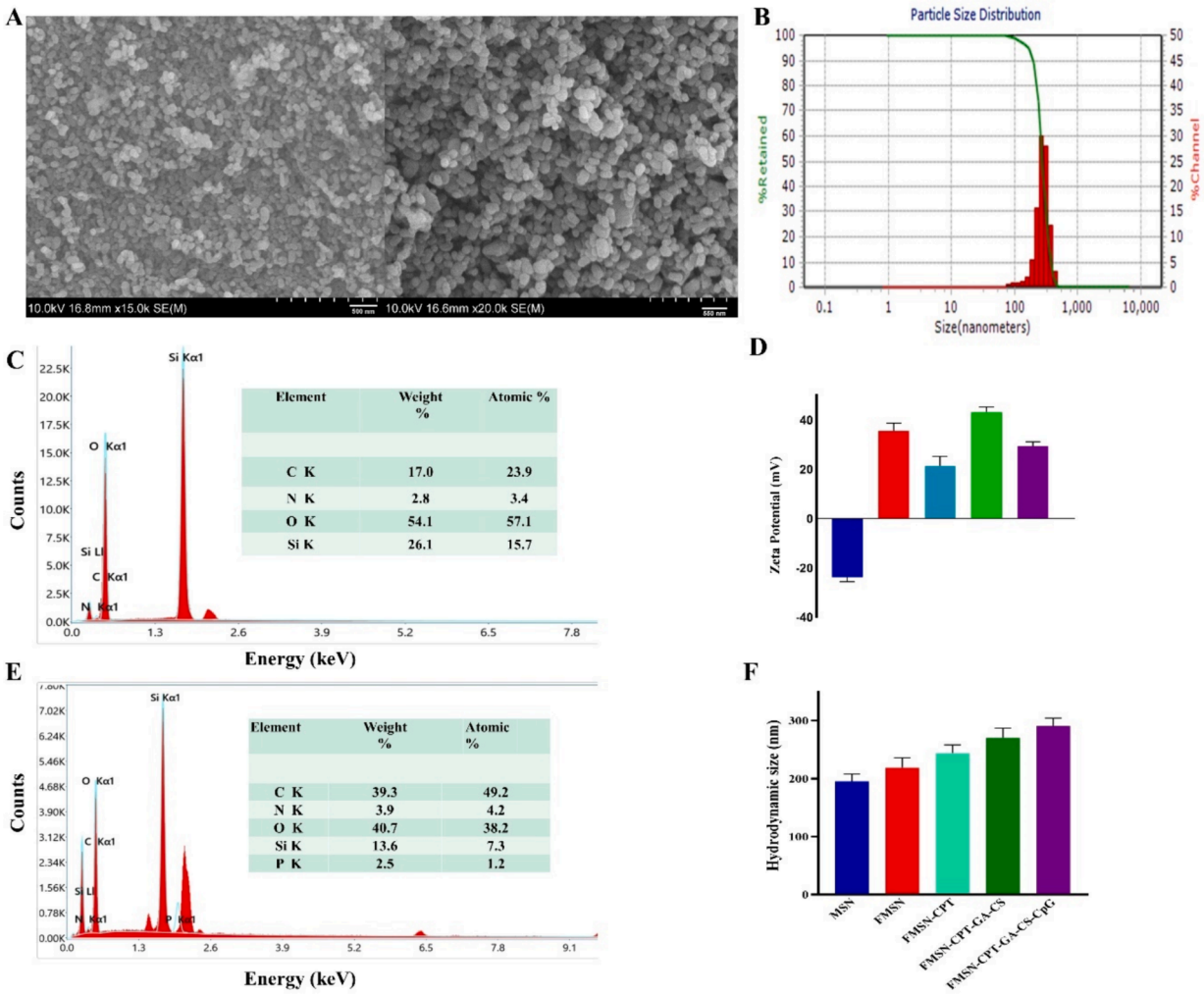

Fig. 2. Physical characterization of NPs (A) Scanning Electron Microscopy (SEM) images (B) Hydrodynamic size distribution (C) Energy-dispersive X-ray spectroscopy (EDX) of FMSN-CPT (D) EDX with CpG ODN (E) Zeta potential and (F) Hydrodynamic size.

due to the presence of NH_2 groups. The electrostatic interaction between the negatively charged CpG and positively charged CS results in a reduction in the overall charge (Iswanti et al., 2019). The PDI of all types of NPs was retained from 0.3 to 0.66. Fig. 2B shows the uniformity of the hydrodynamic size of the prepared NPs. A single sharp and prominent peak signifies the synthesis of uniformly distributed NPs. An alternate shift in the zeta potential after each step illustrates the conversion of MSNs to the end product FMSN-CPT-CS-CpG (Fig. 2, Table 1).

3.3. Scanning Electron microscopy (SEM)

SEM characterization was performed to assess the dry size of NPs. Approximately 50 NPs were chosen and evaluated using the ImageJ software. The bare MSNs presented a uniform, slightly rod-shaped morphology, which can be classified as MCM-41, as shown in Fig. 2A. The observed sizes of the FMSNs and CPT-loaded FMSNs were 180 nm and 205 nm, respectively (Table 1). In contrast, coating NPs resulted in a slightly rough morphology with well-segregated particles and a slightly larger size (235 nm) compared to the uncoated counterparts, owing to the additional CS layer. A comparison of the DLS and SEM analyses is presented in Table 1. However, the deviation of the microscopy results from the DLS study results could be attributed to swollen NPs. Since the DLS method was applied in the liquid phase, it showed a larger mean hydrodynamic particle size compared with SEM, which is the diameter of the dried NPs. The EDX spectrum revealed the presence of Si, C, N, and O (Fig. 2C) in the samples from all groups. The addition of CpG resulted in the appearance of phosphate signals (Fig. 2D), confirming the presence of ODN on the surface of the NPs.

Table 1
Hydrodynamic size, SEM size, Zeta potential, and PdI of NPs.

	Hydrodynamic size (nm)	SEM size (nm)	Zeta potential (mV)	PDI
MSN	195 ± 6.4	167 ± 2.2	–23.7 ± 1.4	0.211
FMSN	211 ± 9.0	180 ± 5.4	+35.50 ± 1.7	0.413
FMSN-CPT	244 ± 7.5	205 ± 4.1	+21.67 ± 2.1	0.426
FMSN-CPT-GA-CS	269 ± 9.1	235 ± 5.3	+43.63 ± 1.2	0.533
FMSN-CPT-GA-CS-CpG	291 ± 5.3	241 ± 3.6	+29.83 ± 0.9	0.316

3.4. Brunauer-Emmett-Teller (BET) surface area analysis

Brunauer-Emmett-Teller (BET) surface area analysis was conducted to evaluate the surface areas and pores. The recorded surface area of bare MSNs was 735.58 m2/g, indicating that MSNs have a large available surface area for the efficient adsorption and loading of guest molecules. The nitrogen adsorption curve of MSN was identified as the typical type IV isotherms according to the IUPAC classification, which is characteristic of mesoporous materials (Babaei et al., 2020). Higher

quantity of adsorption typically indicates a larger surface area available for gas adsorption. The highest curve of blank MSNs among the three materials (Fig. 3A), suggests that they have the most space available for gas molecules to adhere to their surface, compared to FMSN-CPT and FMSN-CPT-GA-CS-CpG.

The pore size measured using the BET method was 7–13 nm and the pore volume measured using the Density Functional Theory (DFT) method was 0.91 cm^3/g (Fig. 3A). After the drug loading, CS coating and binding of CpG ODN, the surface area was reduced to 357.00 m^2/g while the pore volume decreased from 0.91 cm^3/g to 0.57 cm^3/g as shown in (Fig. 3A, Table 2). This reduction could be attributed to the successful incorporation of the drug and the subsequent CS coating of the FMSNs. The drug and CS layers occupy the surface, leading to a reduction in the total available surface area.

Table 2
Surface characterization of NDDS showing the surface area, pore volume, and pore size.

	Surface area (m^2/g)	Pore volume (cm^3/g)	Pore dm (nm)
MSN	735.58	0.91	7–13
FMSN-CPT-GA-CS-CpG	357.00	0.57	-

3.5. Thermogravimetric analysis (TGA)

To evaluate the thermal behavior (Δw %) and extent of surface modification of MSNs, TGA was conducted at a heating rate of 10 °C min^{-1} to 700 °C, as shown in Fig. 3B. All the curves typically exhibit a two-step weight loss. The first weight loss below 150 °C can be ascribed to adsorbed water molecules, condensation of surface silanol groups (Si-OH), and evaporation of the remaining solvent (Dau et al., 2021). Weight loss above 150 °C could be attributed to surface modifications, including APTES functionalization, CPT loading, GA linking, CS coating, and CpG binding, indicating the detachment of particular groups at their respective degradation temperatures. Between 150–700 °C, FMSN lost almost 12.72 % of its weight, which indicates the total decomposition of the NH_2 groups attached to its surface. FMSN-CPT lost 12.28 % within 150 °C and 700 °C, of which 3.24 % (190 °C −310 °C) could be attributed to weight % of CPT. The remaining weight percentage can be considered as the total weight of the MSNs. The differences in Δw % among all the groups are shown in Fig. 3B. The weight loss increased to 27 % after CS coating, indicating that the weight percentage of CS and the weight further decreased to 31 % and 35.5 % for the CS coating with GA crosslinking and after CpG binding, respectively. The curves with GA were observed more stable below 200 °C (Fig. 3B) owing to the cross-linking ability of GA, which can enhance the stability and mechanical strength of CS coating.

3.6. Fourier-Transform Infrared spectroscopy (FTIR)

The fabrication of MSN and the changes in chemical bonding after each step were investigated using FTIR spectroscopy (Fig. 3C and 3D.). The characteristic absorption peaks of MSN appeared at 945 cm^{-1},1045 cm^{-1} and a wide band at 3000 cm^{-1}–3700 cm^{-1}. These peaks can be assigned to the asymmetric vibration of Si-OH, the stretching vibrations of Si-O-Si, and hydrogen-bonded water molecules (Takahashi et al., 2018). The presence of the NH_2 group after APTES modification was confirmed by the N–H stretching bands detected at 3200–3500 cm^{-1}, NH_2 bending at around 1652 cm^{-1} and C-N stretching vibrations at 1200–1300 cm^{-1}. The APTES modification could also be verified by the appearance of peaks at 2997 cm^{-1} and 2933 cm^{-1}, related to the stretching vibration of C–H bond in the propyl chain of APTES (Sun et al., 2019) (Fig. 3C).

The loading of CPT to FMSN displayed changes in the intensity and shapes of certain peaks, including peaks that are typical of esters

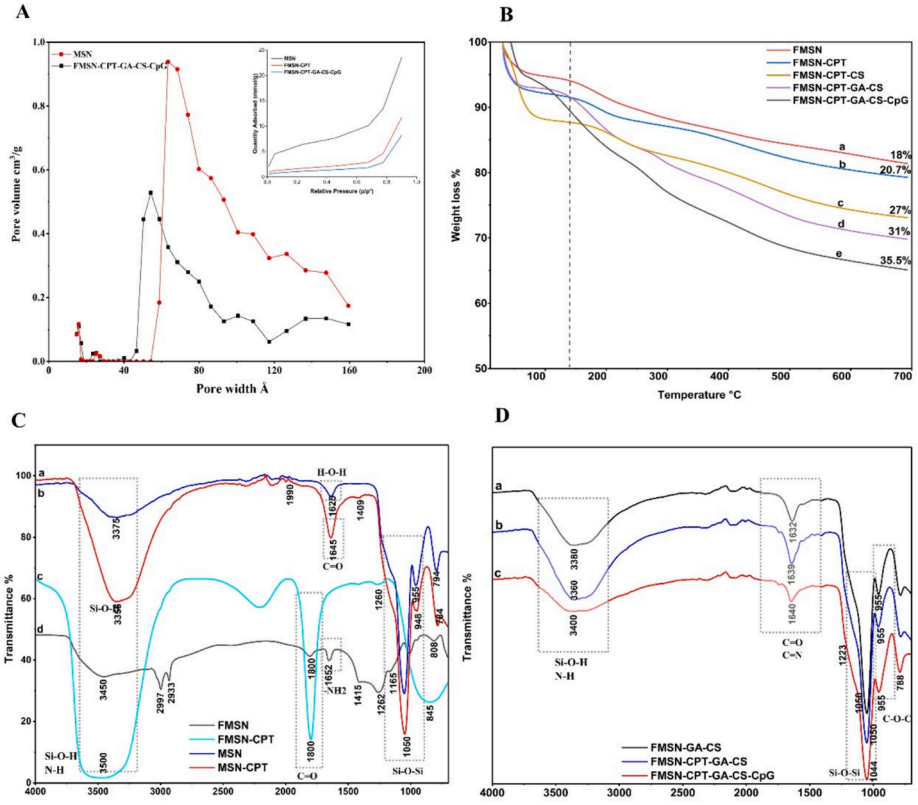

Fig. 3. (A) Brunauer-Emmett-Teller (BET) surface characterization (B) Thermogravimetric Analysis TGA thermal behavior of NPs (C, D) Fourier-Transform Infrared Spectroscopy (FTIR), Chemical characterization.

(organic compounds that have a carbonyl group (C = O) and –OH). The bands related to the Si-OH stretching vibrations at approximately 3755 cm^{-1} exhibited a change in intensity. The peak at approximately 1640 cm^{-1} is likely due to the stretching of the C = O bond, whereas the peak at approximately 3200–3400 cm^{-1} is likely due to the stretching of the O–H bond. The peaks at approximately 1600–1500 cm^{-1} were attributed to the vibrations of the carbon–carbon double bonds (C = C) in the rings (Carrera Espinoza et al., 2021; Subramanian et al., 2011). The presence of NH_2 groups on the surface of the FMSNs allowed potential interactions with CPT (Fig. 3C). Bands typically related to CS can be observed after CS coating. The peaks at 3300–3500 cm^{-1} correspond to the O–H stretching vibrations (Jackson et al., 2023) due to the interaction between the OH groups in CS and FMSN (Fig. 3D), suggesting the presence of H bonding between the two materials. The peaks at 1640 cm^{-1} and 946–960 cm^{-1} are associated with the stretching vibrations of amide bonds and the vibration of the C-O-C bonds (Heidari et al., 2021; Santoso et al., 2019). The bands in the region 1600–1700 cm^{-1} specify the presence of imine bonds (C = N) due to the interaction of GA with the NH_2 groups in CS (Chen and Zhu, 2012; Shah and Rajput, 2018) (Fig. 3D). This suggests a successful cross-linking reaction between GA and CS. The presence of CpG can modify CS-specific bands in the FTIR spectrum. CpG contains phosphate groups, which typically show peaks at 1200 cm^{-1} –1300 cm^{-1} and 1096 cm^{-1} that are overlapped by sharp peaks of characteristic MSN peaks at 980 cm^{-1} to 1280 cm^{-1} (Tao et al., 2015; Xu et al., 2015) (Fig. 3C,D). The FTIR spectra confirmed the successful fabrication of MSNs, functionalization, drug loading, and CS coating.

3.7. Drug loading

The hydrophobic anticancer drug, CPT, was loaded into the nanocarrier. DMSO was chosen as the solvent to maximize drug loading, owing to the hydrophobicity of CPT. The pores of MSN can accommodate both hydrophobic and hydrophilic molecules, making them highly versatile for biomedical and pharmaceutical applications. The drug incorporation efficiency of CPT into MSN, FMSN, and CS-coated FMSN was evaluated using UV spectrophotometry. The drug loading capacity (DLC%) of MSN-OH was 3.24 % out of 5 % and the drug entrapment efficiency (EE%) was 64.8 %, whereas FMSN showed a DLC% of 4.2 % and an EE% of 84 % (Table 3). The obtained results confirm that both MSN-OH and FMSN are capable of effectively loading CPT. However, FMSN showed a higher drug loading capacity and better entrapment efficiency, suggesting that the presence of NH_2 groups on the MSN surface enhances the drug loading process because of electrostatic interactions between the positively charged NH_2 groups and the reactive sites on CPT. These findings are consistent with those of previous studies on the loading of CPT into MSN and FMSN (Llinàs et al., 2018; Lu et al., 2007; Raina et al., 2023). The CS coating on the surface, with or without the incorporation of GA, further improved the drug loading. DLC % and EE% calculated for CS-coated FMSN were 4.5 % and 90 %, respectively, while those for crosslinking were 4.75 % and 95 %, respectively. The UV spectrum (Fig. 4A) shows that the incorporation of GA crosslinking in CS-coated MSNs possibly caused a slight improvement in drug loading, probably because of the increased stability of the CS coating and reduced drug leakage during the loading and washing process, which has also been reported in other studies (Shakeran et al., 2021). The DLC% and EE % of all the NPs groups are presented in Table 3. The average yield of NPs was 80 mg/mL, with a maximum drug loading of 4.75 % for FMSN-CPT-GA-CS. This means 5 mg of NPs could retain almost 0.23 mg of CPT.

Table 3
The DLC% and EE% of all the NPs of all groups.

Sample	DLC (%)	EE (%)
MSN-CPT	3.24 ± 0.3	64.8 ± 0.27
FMSN-CPT	4.15 ± 0.1	84.0 ± 0.14
FMSN-CPT-CS	4.50 ± 0.07	90.0 ± 0.1
FMSN-CPT-GA-CS	4.75 ± 0.08	95.0 ± 0.09

CpG ODN binding to the nanocarrier was detected using a UV spectrophotometer (Fig. 4B).

FMSNs were used as blank to avoid background signals. Free CpG ODN exhibited a characteristic ODN band with the highest intensity at approximately 260 nm (Fig. 4B) and CpG ODN attached to NPs showed a peak a little ahead due to interaction with CS, as shown in Fig.4B. 81 % CpG ODN were detected, and the rest were either washed away or could not bind, and thus could not be detected. CpG ODNs, owing to the phosphate groups in their backbone, carry a negative charge and interact with the positively charged (NH_2) of the CS layer on FMSN via electrostatic interactions. Hydrogen bonding between CS and CpG also facilitated binding, thereby improving the stability of the complex.

3.8. In vitro drug release

An *in vitro* drug release study was performed to evaluate the applicability of FMSNs as carriers for the delivery of hydrophobic drugs. The release pattern of drugs from NDDS is influenced by several factors, such as the chemical and molecular properties of the NPs surface, the physicochemical properties of the encapsulated drug, and the pH of the release media (Chehelgerdi et al., 2023; Zhang et al., 2010). Drug release assays were carried out in PBS at pH 7.4 and pH 6.4 at 37 °C, mimicking physiological and tumor microenvironment (Zhang et al., 2010).

The release profile displayed an initial burst release during the first 6 h at both pH values from all groups (Fig. 4C, D, E), likely due to drug adsorption on the NPs surface (Botella et al., 2011; Llinàs et al., 2018). All CPT molecules from the free CPT group were released into the release medium within 24 h. MSN-OH exhibited an initial burst release (50 %) within the first 8 h, followed by a sustained release phase throughout 48 h, and cumulative drug release reached 85 % within 72 hrs. 65 % of the drug was released from FMSN-CPT within 120 h. CPT release from MSN-CPT and FMSN-CPT was not affected, particularly by changes in pH (Fig. 4C,4D), whereas a significant difference was noted in the drug release patterns of the CS-coated group over 120 h. FMSN-CPT-GA-CS released approximately 51 % and 20 % of its loaded CPT at pH 6.4 and 7.4, respectively. This slow and sustained release profile can be explained by the fact that CS-coated FMSN were significantly affected by pH, which shows that CS is a pH-sensitive polymer that is dependent on the nature of the environment (acidic or neutral) to release the drugs. At pH 6.4, the NH_2 groups of FMSN and OH of CPT were protonated, resulting in repulsive interactions between the positive charges, followed by swelling and pore opening, leading to higher drug release (Botella et al., 2011; Lu et al., 2007). However, after moving away from the acidic pH, it contracted, forming a film that shielded the pores and revealed a significant reduction in CPT release at higher pH (Jackson et al., 2023). Thus, CS, a pH-responsive polymer, provided a sustained CPT release over time. The release of CpG ODN was also found to be pH-dependent and was faster at pH 6.4, probably due to the increased hydrophilicity of CpG ODNs under acidic conditions (Fig. 4E). This release was faster than that of CPT, possibly due to its hydrophilicity and attachment to the outer surface. The rapid initial release was also observed for CpG ODN during the first 6 h, followed by the controlled release that reached 60 % in 60 h at pH 6.4. Other studies have also found almost the same release curves for CpG ODN bound to cationic polymers (Chen et al., 2013; Zhang et al., 2019). Thus, the rate of release is inversely proportional to the pH of the external medium, which means that it increases with a decrease in pH. A small amount of CPT and CpG released under normal physiological conditions (pH 7.4) indicates that NDDS is well protected from drug release to normal tissues, which is essential for limiting the high toxicity of these drugs to healthy cells (Huarte et al., 2016). This also suggests the possibility of prolonging the therapeutic effects of the drug and reducing its administration frequency.

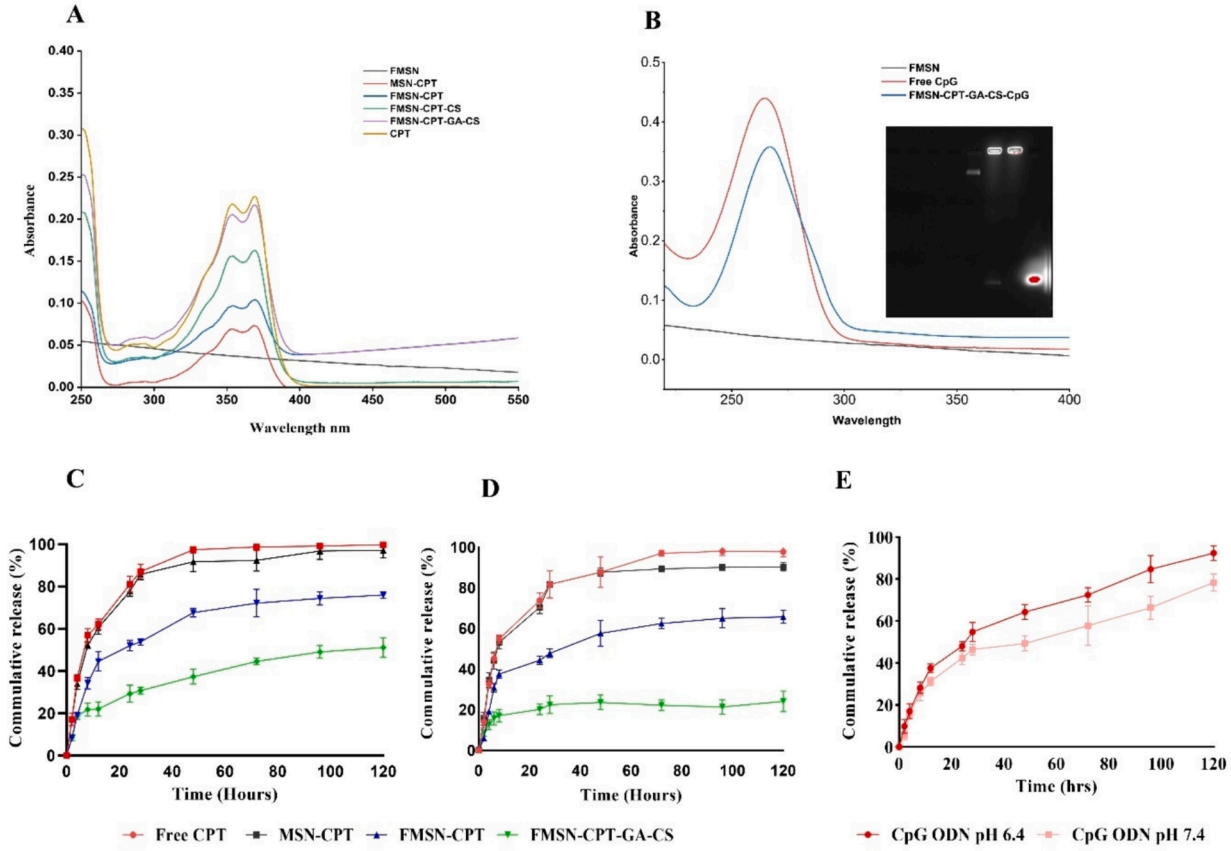

Fig. 4. (A) UV spectrum of CPT, blank FMSN, MSN-CPT, FMSN-CPT, FMSN-CPT-CS, FMSN-CPT-GA-CS (B) UV spectrum of CpG ODN and gel electrophoresis detection of CpG ODN (C, D) Cumulative release of CPT, MSN-CPT, FMSN-CPT and FMSN-CPT-GA-CS at pH 6.4 and pH 7.4, respectively, (E) Cumulative CpG ODN release at pH 6.4 and pH 7.4.

3.9. In vitro cytotoxicity

An MTT assay was conducted to evaluate the cytotoxicity of the NPs formulations and to evaluate the synergism of CPT and CpG ODN when delivered together as a targeted NDDS against B16F10 cells. The cytocompatibility of bare MSN, FMSN, and CS-coated FMSN is well established against many other cancer cell lines, including MCF7 (Shakeran et al., 2021), CHO (Babaei et al., 2020; Lin et al., 2018), C26 (Babaei et al., 2020), 3 T3 (Daryasari et al., 2016), HepG2 (Fu et al., 2022), Glioblastoma and U87 MG cells (Householder et al., 2015). Only one study was performed on B16F10 cells, where MSN-CPT was coated with poly(ethylene glycol)-poly(b-aminoester urethane) (PAEU) and delivered in the form of a hydrogel, either alone or in combination with doxorubicin (Min et al., 2023). Herein, we demonstrated the cytocompatibility of blank MSNs, FMSNs, and CS-coated FMSNs and the cytotoxicity of CPT-loaded FMSN against B16F10 cells. When treated with blank FMSN and FMSN-CS, 84 % (FMSN-CS) and 77 % (FMSN) of cells were viable at 800 μg/mL even after 48 h of incubation (Fig. 5B), which confirmed that the blank NPs exhibited good biocompatibility and that the CS coating further enhanced biocompatibility due to the shielding effect of CS.

Next, we evaluated the concentration-dependent responses of B16F10 cells to various formulations, including free CPT, FMSN-CPT, FMSN-CPT-GA-CS, and FMSN-CPT-GA-CS-CpG, incubated at 37 °C for 48 h. The results revealed that free CPT and FMSN-CPT exhibited comparable cell-killing potency, with no statistically significant difference, as shown in Fig. 5C. Free CPT displayed slightly enhanced cytotoxicity owing to its efficient release compared to FMSN-CPT. However, the addition of CS to FMSN-CPT resulted in a reduction in cell viability compared to free CPT and FMSN-CPT (Fig. 5C) because of an additional positively charged CS layer on the surface that could interact with the negatively charged cell membrane, accumulating inside or around the cell, influencing the drug release kinetics (pH-dependent) and releasing the drug within the cancerous cell (slightly acidic). The binding of CpG ODN to the surface of CPT-loaded FMSN vividly exhibited exceptionally high cytotoxicity, with only 10 % viable cells remaining after 48 h at 7 mM concentration ($p < 0.00001$). Time dependent analysis was conducted to evaluate the drug release from the nanocarrier over time. As shown in Fig. 5D, a long incubation time was required for drug release from FMSN-CPT and FMSN-CPT-GA-CS to display its cytotoxic effect (Fig. 5D); however, free CPT was more toxic because of its quick release, while the distribution of drug-loaded nanocarriers increased cytotoxicity over time. After 24 h, FMSN-CPT-GA-CS significantly reduced cell viability compared to free CPT ($p = 0.0001$). After 72 h of incubation, FMSN-CPT and FMSN-CPT-GA-CS showed reduced cell viability compared with free CPT, which could be attributed to the slow and sustained release of CPT from the pores of the nanocarrier. FMSN-CPT-GA-CS-CpG showed significantly lower ($p = 0.0003$) viable cells (15 %) than the other groups after 72 h (Fig. 5D). This significantly heightened cytotoxicity upon co-delivery of CPT with CpG ODN, emphasizing the synergistic potential of this multifunctional NDDS. CpG ODN stimulates the immune response by activating Toll-like receptor 9 (TLR9), resulting in improved recognition, cellular uptake, and localized/targeted release of CpG ODN and CPT into cancer cells, leading to more potent and sustained therapeutic efficacy as compared to their free counterparts.

3.10. Cutaneous chemical carcinogenesis and in vivo anticancer potential

To investigate the antitumor efficacy of the formulated NPs, a tumor model was developed using DMBA/TPA in BALB/c mice. Tumors with a

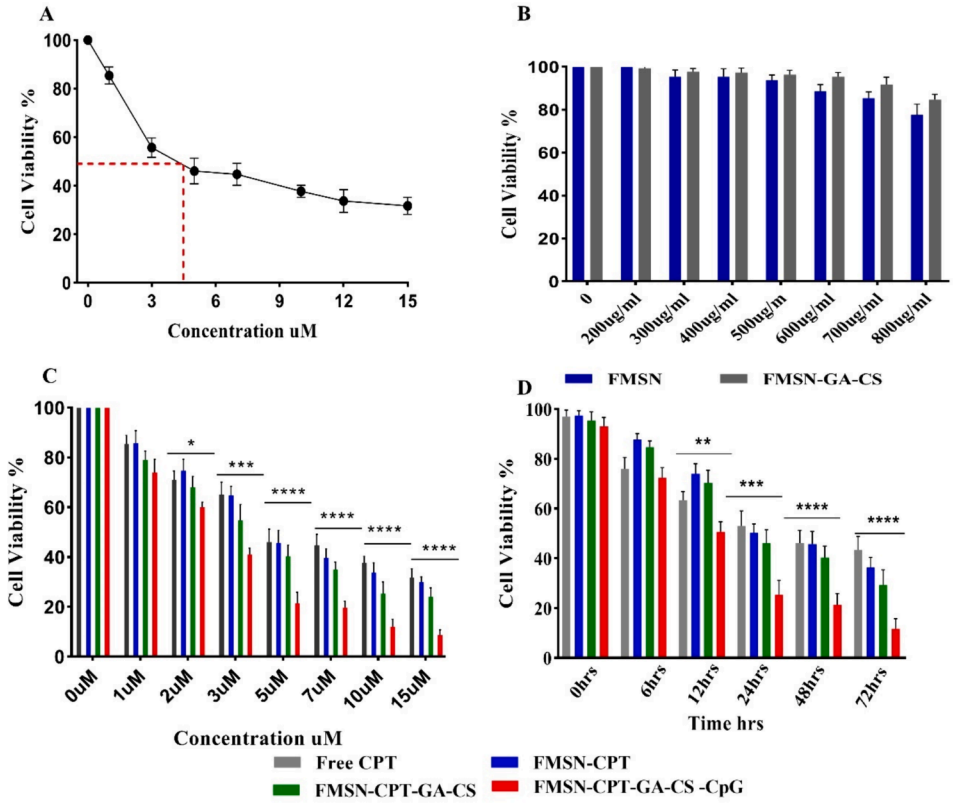

Fig. 5. *In vitro* cytotoxicity of formulated NDDS against B16F10 cells, the drug was used as 5 % of the carrier in all groups. $p-$ value >0.05 represents not significant (ns), $p-$ value ≤ 0.05 represents significance (*), $p-$ value ≤ 0.01 (**), $p-$ value ≤ 0.001 (***) and $p-$ value ≤ 0.0001 (****) (A) Cell viability % against free CPT (B) Cytocompatibility of blank FMSNs in increasing concentrations (C) Concentration dependent cytotoxicity for 48 h (D) Time dependent cytotoxicity at a concentration of 5 μM.

minimum size of 3 mm that did not regress for two weeks were considered for treatment. Established tumors were treated locally via intratumoral injections of PBS, free CPT, FMSN-CPT, or FMSN.CPT-GA-CSand FMSN-CPT-GA-CS-CpG. Systemic toxicity in each group was assessed by monitoring the body weight and survival rates following the respective formulations. Distinct trends were observed among the treatment groups. A decline in body weight was observed in the animals treated with free CPT.

One mouse died within 24 h and 48 h following injection, after each dose of free CPT, which can be ascribed to the late systemic toxicity of free CPT, as reported previously (Fehér, 2019; Momin et al., 2022). Moreover, free CPT initially demonstrated a reduction in papillomas following two to four days post-injection; however, the papillomas aggressively regrown until the second dose. This could be attributed to the instability of the free drug in the plasma, leading to conversion of the active lactone ring of CPT into the carboxylate form (inactive) [31]. Animals treated with FMSN-CPT displayed a similar regression trend but a slight delay in tumor regrowth. Notably, FMSN-CPT-GA-CS treatment resulted in significantly fewer tumors than the free CPT and FMSN-CPT treated groups, suggesting a potential impact of the CS coating in inhibiting tumors by adhering to the negatively charged dermal cells via strong electrostatic interactions. Furthermore, encapsulation and coating can prevent deactivation of the drug, enhance cellular uptake, and subsequently improve its effectiveness. Numerous studies have confirmed enhanced dermal penetration and improved efficacy of drugs due to the presence of a CS coating (Campos et al., 2022; Jafernik et al., 2023; Nhavene et al., 2018). Most strikingly, the FMSN-CPT-CS-CpG group displayed an exceptional decrease in papillomas for two weeks, and papillomas did not show aggressive regrowth, even in the absence of injection. This effect persisted for 20 weeks until the end of the experiment (Fig. 6B, C, D). This *in vivo* synergism of CPT with CpG ODN in the form of FMSN-CPT-GA-CS-CpG was evident compared to control groups, validating the advantages of combination treatment in the murine SCC model as the reduction in the cumulative number of tumors; post-treatment was much more pronounced with 100 % survival (Fig. 6D). Furthermore, administration of drugs via intratumoral injection offers the major advantage of reducing systemic exposure by maintaining the maximum therapeutic concentration within the tumor microenvironment, showing immediate tumor responses, and facilitating controlled modulation of local immune cascades (Lai et al., 2019). This treatment combination has also been reported in PDVC57 tumors when treated with either non-adhesive or bioadhesive NPs of CPT alone or in combination with CpG ODN, which improved the percent survival relative to controls and single therapy, revealing the potential of local tumor synergistic immunotherapy (J. K. Hu et al., 2021). We also found that codelivery of an adjuvant immunosensitizing agent, CpG ODN, may augment the efficacy of FMSN-CPT-CS in eliminating tumors and prolonging animal survival (100 %) by stimulating a local immune response to treatment, which is also supported by previous reports where CpG as a TLR9 ligand-activated immune response when used with chemotherapy and radiotherapy against cutaneous malignancies (Appelbe et al., 2017; Fehér, 2019; Lai et al., 2019).

3.11. Histopathological evaluation

Histological (H&E staining) examination of the mouse skin from all groups was conducted to assess the internal morphology of the tumor tissues. The negative control exhibited a well-defined epidermal morphology with underlying dermis and subcutaneous tissue (Fig. 7B, a). DMBA/TPA resulted in ulceration with well-developed hyperchromatia, thickened corrugated epidermis, and hyperkeratosis as key features. Upon synergistic treatment with local chemotherapy and

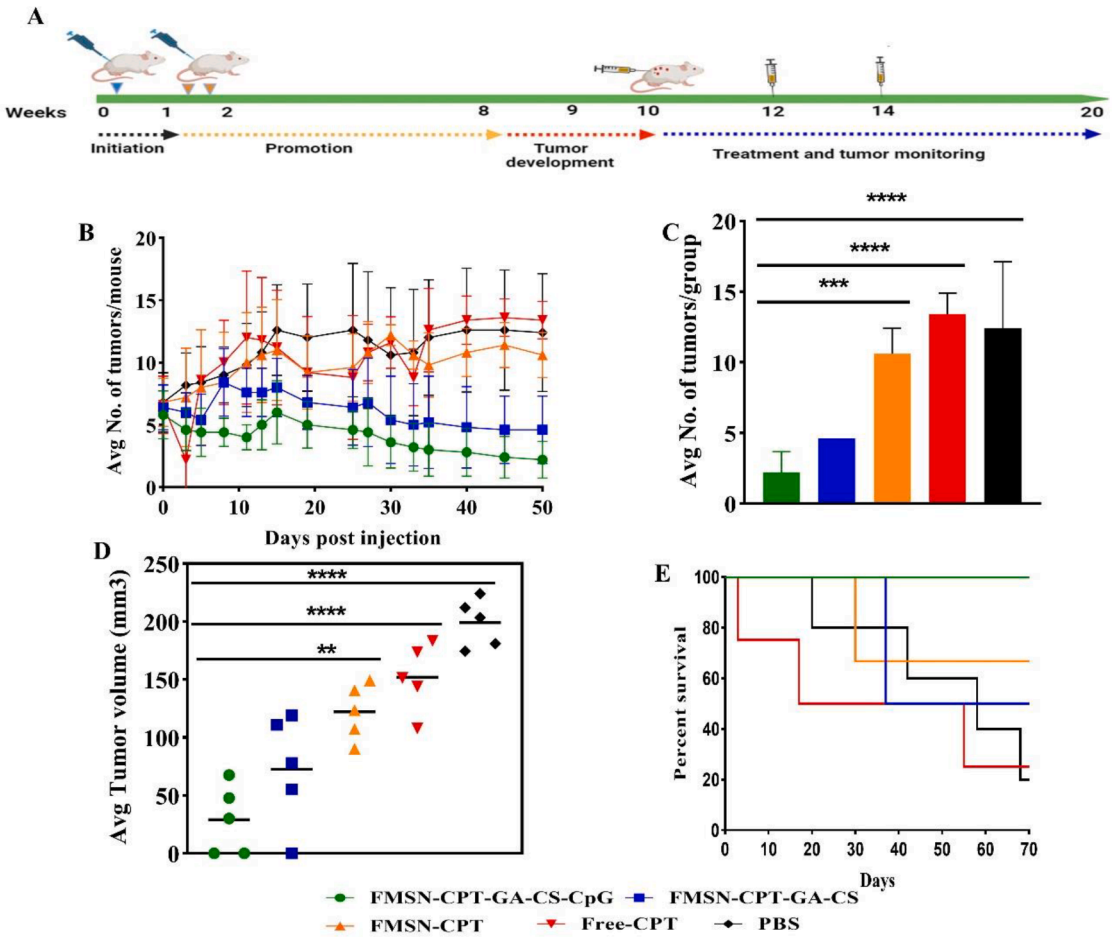

Fig. 6. *In vivo* tumor killing in murine model, p − value > 0.05 represents not significant (ns), p − value ≤ 0.05 represents significance (*), p − value ≤ 0.01 (**), p − value ≤ 0.001 (***) and p − value ≤ 0.0001 (****) (A) treatment schedule, initiation by DMBA, promotion by TPA followed by NPs injection at week 10, CPT dose of 0.25 mg/mouse, distributed into tumors via intratumoral injections depending on tumor size (B) Average number of tumors per mouse post treatment (C) Average number of tumors per group at the end of study showing the comparison of FMSN-CPT-GA-CS-CpG group with FMSN-CPT-GA-CS (p = ns), FMSN-CPT ($p \leq 0.001$), free CPT ($p \leq 0.0001$), and DMBA/TPA ($p \leq 0.0001$), (D) Average tumor volume showing significant difference between FMSN-CPT-GA-CS-CpG and FMSN-CPT, free CPT ($p \leq 0.0001$), and DMBA/TPA group ($p \leq 0.0001$), (E) Kaplan-Meier curve showing percent survival of all treatment groups.

adjuvant immunotherapy, the tumor burden substantially decreased. The skin had an intact epidermis and an average deep dermis with mild inflammation (Fig. 7A, a,b, and Fig. 7B,c).

4. Conclusion

Our study demonstrates the successful development of a multifaceted NDDS that effectively delivered the hydrophobic, anticancer drug, CPT to skin cancer cells, exhibiting remarkable efficacy both *in vitro* and *in vivo* preclinical studies. The CS coating contributed to the sustained and pH-dependent release of CPT because of the pH-responsiveness of CS, as the release was faster at an acidic pH (tumor microenvironment) than at a neutral pH (normal physiological pH). The incorporation of CpG ODN into the NDDS serves to immunostimulate the local chemotherapy, amplifying the therapeutic impact significantly, leading to a remarkable synergistic effect both *in vitro* in B16F10 cells and the pronounced tumor regression *in vivo* in DMBA/TPA-induced SCC in a murine model. The formulation's success is particularly notable given the poor stability of free CpG ODN, which limits its clinical applications. However, binding it to the surface of aminated NPs can substantially improve its stability. The findings propose that the combined localized anticancer strategy without resorting to surgical approaches, holds great potential for enhanced skin cancer therapy, paving the way for future advancements in NDDS based synergistic therapies for cutaneous malignancies. The efficacy of local (intratumoral) injections in delivering NDDS to the tumor site, with minimal distribution to nontarget areas underscores the need for additional studies to validate this delivery method fully. Furthermore, comprehensive research with a large sample size is required to completely explore the immune cascade involved in combination therapy and the underlying molecular mechanisms. Determining whether local treatment provides efficacy in the clinical setting and whether response rates would approach those of intravenous or orally delivered agents also requires additional clinical studies.

CRediT authorship contribution statement

Munibah Qureshi: Writing – original draft, Investigation. **Cláudia Viegas:** Validation, Data curation. **Sofia O.D. Duarte:** Writing – review & editing, Validation, Formal analysis. **Michael Girardi:** Writing – review & editing, Supervision, Funding acquisition, Conceptualization. **Adeeb Shehzad:** Writing – review & editing, Supervision, Resources, Funding acquisition, Conceptualization. **Pedro Fonte:** Writing – review & editing, Validation, Resources, Project administration, Funding acquisition, Conceptualization.

Declaration of competing interest

The authors declare that they have no known competing financial interests or personal relationships that could have appeared to influence the work reported in this paper.

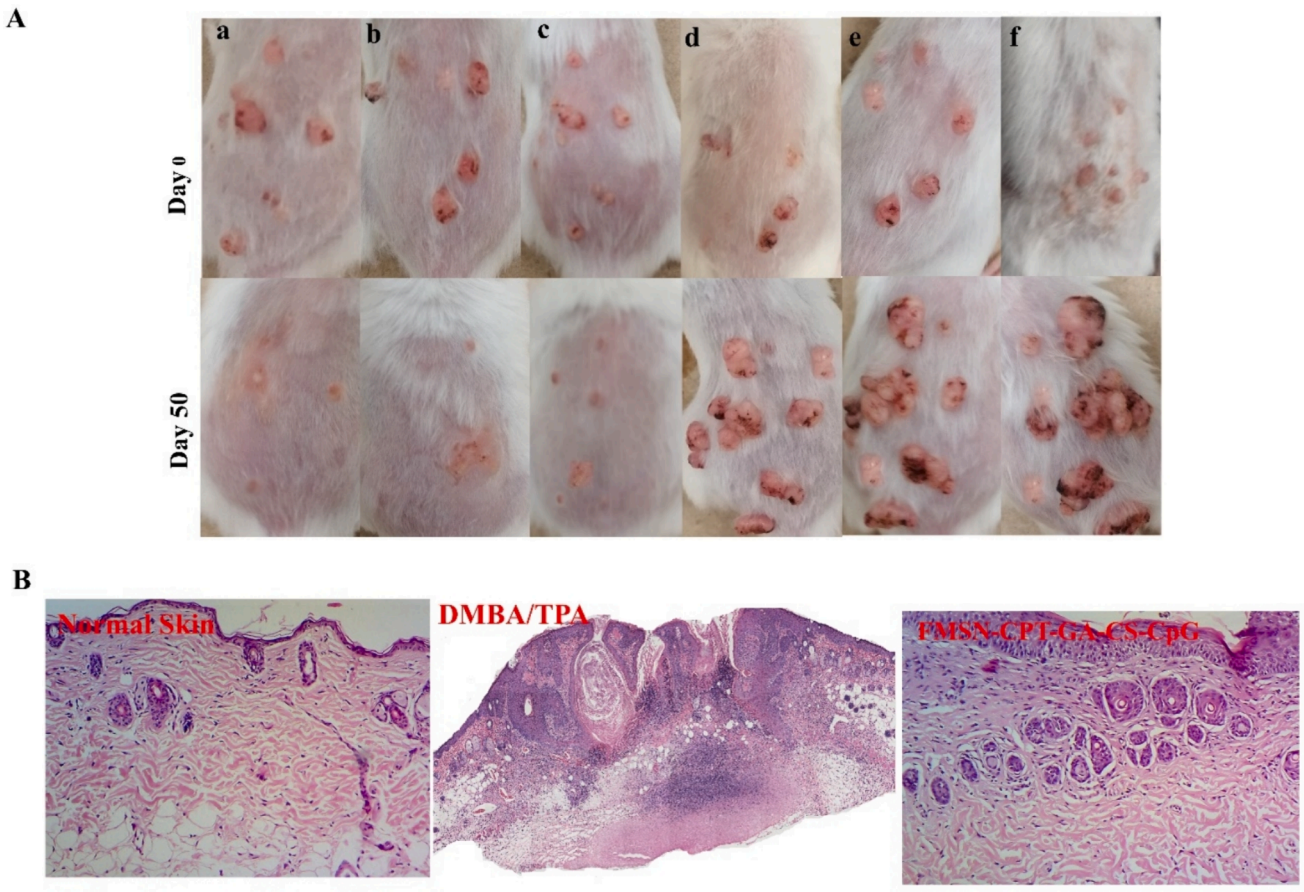

Fig. 7. (A) Mice papillomas at day 0 of intratumoral injections and at day 50 (a) FMSN-CPT-GA-CS-CpG (b) FMSN-CPT-GA-CS-CpG (c) FMSN-CPT-GA-CS (d) FMSN-CPT (e) Free CPT (f) PBS. (B) H & E staining of normal mouse skin, skin treated with FMSN-CPT-GA-CS-CpG, and only DMBA/TPA treated skin after 20 weeks.

Data availability

Data will be made available on request.

Acknowledgments

The authors acknowledge Fundação para a Ciência e a Tecnologia (FCT), Portugal in the scope of the projects UIDB/04326/2020 (DOI:10.54499/UIDB/04326/2020), UIDP/04326/2020 (DOI:10.54499/UIDP/04326/2020), and LA/P/0101/2020 (DOI:10.54499/LA/P/0101/2020) of the Research Unit Center for Marine Sciences—CCMAR, and UIDB/04565/2020 (DOI:10.54499/UIDB/04565/2020) and UIDP/04565/2020 (DOI:10.54499/UIDP/04565/2020) of the Research Unit Institute for Bioengineering and Biosciences—iBB, and LA/P/0140/2020 (DOI:10.54499/LA/P/0140/2020) of the Associate Laboratory Institute for Health and Bioeconomy—i4HB. Cláudia Viegas also thanks the FCT for the PhD fellowship (2020.08839.BD). Munibah Qureshi acknowledges the Higher Education Commission (HEC) of Pakistan for providing research support for this study. We also thank Dr Muhammad Rafii from the National Institute of Lasers and Optronics (NILOP) College, Islamabad, Pakistan for his generous support and providing lab services.

Appendix A. Supplementary material

Supplementary data to this article can be found online at https://doi.org/10.1016/j.ijpharm.2024.124340.

References

Abasalizadeh, F., Moghaddam, S.V., Alizadeh, E., Akbari, E., Kashani, E., Fazljou, S.M.B., Torbati, M., Akbarzadeh, A., 2020. Alginate-based hydrogels as drug delivery vehicles in cancer treatment and their applications in wound dressing and 3D bioprinting. J. Biol. Eng. 14, 8. https://doi.org/10.1186/s13036-020-0227-7.

Amin, M.U., Ali, S., Ali, M.Y., Fuhrmann, D.C., Tariq, I., Seitz, B.S., Preis, E., Brüßler, J., Brüne, B., Bakowsky, U., 2022. Co-delivery of carbonic anhydrase IX inhibitor and doxorubicin as a promising approach to address hypoxia-induced chemoresistance. Drug Deliv. 29, 2072–2085. https://doi.org/10.1080/10717544.2022.2092234.

Andrade, F., Fonte, P., Oliva, M., Videira, M., Ferreira, D., Sarmento, B., 2015. Solid state formulations composed by amphiphilic polymers for delivery of proteins: Characterization and stability. Int. J. Pharm. 486 https://doi.org/10.1016/j.ijpharm.2015.03.050.

Appelbe, O.K., Moynihan, K.D., Flor, A., Rymut, N., Irvine, D.J., Kron, S.J., 2017. Radiation-enhanced delivery of systemically administered amphiphilic-CpG oligodeoxynucleotide. J. Control. Release 266, 248–255. https://doi.org/10.1016/j.jconrel.2017.09.043.

Babaei, M., Abnous, K., Taghdisi, S.M., Taghavi, S., Sh. Saljooghi, A., Ramezani, M., Alibolandi, M., 2020. Targeted rod-shaped mesoporous silica nanoparticles for the co-delivery of camptothecin and survivin shRNA in to colon adenocarcinoma in vitro and in vivo. Eur. J. Pharm. Biopharm. 156, 84–96. doi: 10.1016/j.ejpb.2020.08.026.

Bayne, K., 2011. Revised Guide for the Care and Use of Laboratory Animals available. American Physiological Society, The National Academies Press.

Botella, P., Abasolo, I., Fernández, Y., Muniesa, C., Miranda, S., Quesada, M., Ruiz, J., Schwartz, S., Corma, A., 2011. Surface-modified silica nanoparticles for tumor-targeted delivery of camptothecin and its biological evaluation. J. Control. Release 156, 246–257. https://doi.org/10.1016/j.jconrel.2011.06.039.

Campos, E.V.R., Proença, P.L.F., Da Costa, T.G., De Lima, R., Fraceto, L.F., De Araujo, D. R., 2022. Using Chitosan-Coated Polymeric Nanoparticles-Thermosensitive Hydrogels in association with Limonene as Skin Drug Delivery Strategy. Biomed Res. 2,1-18. Int. doi: 10.1155/2022/9165443.

Carrera Espinoza, M.J., Lin, K.S., Weng, M.T., Kunene, S.C., Wang, S.-S., S.,, 2021. In vitro studies of Pluronic F127 coated magnetic silica nanocarriers for drug delivery system targeting liver cancer. Eur. Polym. J. 153, 110504 https://doi.org/10.1016/j.eurpolymj.2021.110504.

Castro, P.M., Fonte, P., Oliveira, A., Madureira, A.R., Sarmento, B., Pintado, M.E., 2017. Optimization of two biopolymer-based oral films for the delivery of bioactive

molecules. Mater. Sci. Eng. C. 76, 171–180. https://doi.org/10.1016/j.msec.2017.02.173.
Chehelgerdi, M., Chehelgerdi, M., Allela, O.Q.B., Pecho, R.D.C., Jayasankar, N., Rao, D. P., Thamaraikani, T., Vasanthan, M., Viktor, P., Lakshmaiya, N., Saadh, M.J., Amajd, A., Abo-Zaid, M.A., Castillo-Acobo, R.Y., Ismail, A.H., Amin, A.H., Akhavan-Sigari, R., 2023. Progressing nanotechnology to improve targeted cancer treatment: overcoming hurdles in its clinical implementation. Mol. Cancer. 22, 1476–4598. https://doi.org/10.1186/s12943-023-01865-0.
Chen, S., Zhang, H., Chinnathambi, S., Hanagata, N., 2013. Synthesis of novel chitosan-silica/CpG oligodeoxynucleotide nanohybrids with enhanced delivery efficiency. Mater. Sci. Eng. C 33, 3382–3388. https://doi.org/10.1016/j.msec.2013.04.017.
Chen, F., Zhu, Y., 2012. Chitosan enclosed mesoporous silica nanoparticles as drug nanocarriers: Sensitive response to the narrow pH range. Microporous Mesoporous Mater. 150, 83–89. https://doi.org/10.1016/j.micromeso.2011.07.023.
Cheng, Z., Shan, H., Sun, Y., Zhang, L., Jiang, H., Li, C., 2020. Applied Surface Science Evolution mechanism of surface hydroxyl groups of silica during heat treatment. Appl. Surf. Sci. 513, 145766 https://doi.org/10.1016/j.apsusc.2020.145766.
Cho, Y.T., Chen, K.L., Chu, C.Y., 2016. Treatment strategies of epidermal growth factor receptor inhibitorinduced skin toxicities: Pre-emptive or reactive? Ann. Transl. Med. 4, 4–6. https://doi.org/10.21037/atm.2016.08.03.
Choi, E., Kim, S., 2019. Surface pH buffering to promote degradation of mesoporous silica nanoparticles under a physiological condition. J. Colloid Interface Sci. 533, 463–470. https://doi.org/10.1016/j.jcis.2018.08.088.
Cordeiro, R.A., Mendonça, P.V., Coelho, J., Faneca, H., 2022. Engineering silica-polymer hybrid nanosystems for dual drug and gene delivery. Biomater. Adv. 135, 212742 https://doi.org/10.1016/j.bioadv.2022.212742.
Daryasari, M.P., Akhgar, M.R., Mamashli, F., Bigdeli, B., Khoobi, M., 2016. Chitosan-folate coated mesoporous silica nanoparticles as a smart and pH-sensitive system for curcumin delivery. RSC Adv. 6, 105578–105588. https://doi.org/10.1039/c6ra23182a.
Dau, T.A.N., Le, V.M.H., Pham, T.K.H., Le, V.H., Cho, S.K., Nguyen, T.N.U., Ta, T.K.H., Van Tran, T.T., 2021. Surface Functionalization of Doxorubicin loaded MCM-41 Mesoporous Silica Nanoparticles by 3-Aminopropyltriethoxysilane for Selective Anticancer 9 Effect on A549 and A549/DOX Cells. J. Electron. Mater. 50, 2932–2939. https://doi.org/10.1007/s11664-021-08813-y.
De Oliveira, L.F., Bouchmella, K., Picco, A.S., Capeletti, L.B., Gonçalves, K.A., Dos Santos, J.H.Z., Kobarg, J., Cardoso, M.B., 2017. Tailored silica nanoparticles surface to increase drug load and enhance bactericidal response. J. Braz. Chem. Soc. 28, 1715–1724. https://doi.org/10.21577/0103-5053.20170017.
Dessinioti, C., Pitoulias, M., A.j.s.,, 2021. Epidemiology of advanced cutaneous squamous cell carcinoma. J. Eur. Acadamey Dermatology Venereol. 36, 39–50. https://doi.org/10.1111/jdv.17709.
Koohi Moftakhari Esfahani, M., Alavi, S.E., Cabot, P.J., Islam, N., Izake, E.L., 2022. Application of mesoporous silica nanoparticles in cancer therapy and delivery of repurposed anthelmintics for cancer therapy. Pharmaceutics 14,1579. doi: 10.3390/pharmaceutics14081579.
Ezoe, S., Palacpac, N.M.Q., Tetsutani, K., Yamamoto, K., Okada, K., Taira, M., Nishida, S., Hirata, H., Ogata, A., Yamada, T., Yagi, M., Edula, J.R., Oishi, Y., Tougan, T., Ishii, K. J., Myoui, A., Horii, T., 2020. First-in-human randomised trial and follow-up study of Plasmodium falciparum blood-stage malaria vaccine BK-SE36 with CpG-ODN(K3). Vaccine. 38, 7246–7257. https://doi.org/10.1016/j.vaccine.2020.09.056.
Fan, D., Cao, Y., Cao, M., Wang, Y., Cao, Y., Gong, T., 2023. Nanomedicine in cancer therapy. Signal Transduct. Target. Ther. 8, 293. https://doi.org/10.1038/s41392-023-01536-y.
Fania, L., Didona, D., Di Pietro, F.R., Verkhovskaia, S., Morese, R., Paolino, G., Donati, M., Ricci, F., Coco, V., Ricci, F., Candi, E., Abeni, D., Dellambra, E., 2021. Cutaneous squamous cell carcinoma: From pathophysiology to novel therapeutic approaches. Biomedicines 9, 1–33. https://doi.org/10.3390/biomedicines9020171.
Fehér, K., 2019. Single Stranded DNA Immune Modulators with Unmethylated CpG Motifs: Structure and Molecular Recognition by Toll-Like Receptor 9. Curr. Protein Pept. Sci. 20, 201731031. https://doi.org/10.2174/1389203720666190830162149.
Fu, C., Qin, J., Liu, X., Kong, F., 2022. Galactosed and Reduction-Responsive Nanoparticles Assembled from Trimethylchitosan–Camptothecin Conjugates for Enhanced Hepatocellular Carcinoma Therapy. 14 1315. doi: 10.3390/pharmaceutics14071315.
Gao, J., Fan, K., Jin, Y., Zhao, L., Wang, Q., Tang, Y., Xu, H., Liu, Z., Wang, S., Lin, J., Lin, D., 2019. PEGylated lipid bilayer coated mesoporous silica nanoparticles co-delivery of paclitaxel and curcumin leads to increased tumor site drug accumulation and reduced tumor burden. Eur. J. Pharm. Sci. 140, 105070 https://doi.org/10.1016/j.ejps.2019.105070.
Gomes, A.S., Correia, A., Rahikkala, A., Mäkilä, E., Pinto, M.M., Sousa, E., Salonen, J., Saraiva, L., Santos, H.A., 2022. Folic acid-mesoporous silicon nanoparticles enhance the anticancer activity of the p73-activating small molecule LEM2. Int. J. Pharm. 624, 121959 https://doi.org/10.1016/j.ijpharm.2022.121959.
Gordon, L.G., Rowell, D., 2015. Health system costs of skin cancer and cost-effectiveness of skin cancer prevention and screening: a systematic review. Eur. J. Cancer Prev. 24, 141–149. https://doi.org/10.1097/CEJ.0000000000000056.
Gustavson, D.E., Miyake, A., 2016. Mesoporous Silica Nanoparticle Delivery of Chemically Modified siRNA Against TWIST1 Leads to Reduced Tumor Burden. Cogn. Emot. J. 30, 1289–1303. https://doi.org/10.1016/j.nano.2015.05.011.
Han, W., Xie, B., Li, Y., Shi, L., Wan, J., Chen, X., Wang, H., 2019. Orally deliverable nanotherapeutics for the synergistic treatment of colitis-associated colorectal cancer. Theranostics 9, 7458–7473. https://doi.org/10.7150/thno.38081.
Heidari, R., Khosravian, P., Mirzaei, S.A., Elahian, F., 2021. siRNA delivery using intelligent chitosan-capped mesoporous silica nanoparticles for overcoming multidrug resistance in malignant carcinoma cells. Sci. Rep. 11, 1–14. https://doi.org/10.1038/s41598-021-00085-0.
Honda-Okubo, Y., Antipov, A., Andre, G., Barati, S., Kafi, H., Petrovsky, N., 2023. Ability of SpikoGen®, an Advax-CpG adjuvanted recombinant spike protein vaccine, to induce cross-neutralising antibodies against SARS-CoV-2 variants. Immunology. 170, 193–201. https://doi.org/10.1111/imm.13661.
Householder, K.T., Diperna, D.M., Chung, E.P., Wohlleb, G.M., Dhruv, H.D., Berens, M. E., Sirianni, R.W., 2015. Intravenous delivery of camptothecin-loaded PLGA nanoparticles for the treatment of intracranial glioma. Int. J. Pharm. 479, 374–380. https://doi.org/10.1016/j.ijpharm.2015.01.002.
Hu, Y., Bai, S., Wu, X., Tan, S., He, Y., 2021b. Biodegradability of mesoporous silica nanoparticles. Ceram. Int. 47, 31031–31041. https://doi.org/10.1016/j.ceramint.2021.08.129.
Hu, J.K., Suh, H.W., Qureshi, M., Lewis, J.M., Yaqoob, S., Moscato, Z.M., Griff, S., Lee, A. K., Yin, E.S., Mark Saltzman, W., Girardi, M., 2021a. Nonsurgical treatment of skin cancer with local delivery of bioadhesive nanoparticles. Proc. Natl. Acad. Sci. U. S. A. 118, 1–8. https://doi.org/10.1073/pnas.2020575118.
Huarte, J., Espuelas, S., Lai, Y., He, B., Tang, J., Irache, J.M., 2016. Oral delivery of camptothecin using cyclodextrin/poly(anhydride) nanoparticles. Int. J. Pharm. 506, 116–128. https://doi.org/10.1016/j.ijpharm.2016.04.045.
Iswanti, F.C., Nurulita, I., Djauzi, S., Witarto, A.B., Yamazaki, T., 2019. Preparation, characterization, and evaluation of chitosan-based nanoparticles as CpG ODN carriers. Biotechnol. Biotechnol. Equip. 33, 390–396. https://doi.org/10.1080/13102818.2019.1578690.
Jackson, N., Ortiz, A.C., Jerez, A., Morales, J., Arriagada, F., 2023. Kinetics and Mechanism of Camptothecin Release from Transferrin-Gated Mesoporous Silica Nanoparticles through a pH-Responsive Surface Linker. Pharmaceutics 15, 1590. https://doi.org/10.3390/pharmaceutics15061590.
Jafernik, K., Ładniak, A., Blicharska, E., Czarnek, K., Ekiert, H., Wiącek, A.E., Szopa, A., 2023. Chitosan-Based Nanoparticles as Effective Drug Delivery Systems—A review. Molecules 28, 1–17. https://doi.org/10.3390/molecules28041963.
Kundu, M., Chatterjee, S., Ghosh, N., Manna, P., Das, J., Sil, P.C., 2020. Tumor targeted delivery of umbelliferone via a smart mesoporous silica nanoparticles controlled-release drug delivery system for increased anticancer efficiency. Materials Science and Engineering C. Elsevier B.v. 116 (111239) https://doi.org/10.1016/j.msec.2020.111239.
Lai, J.C.Y., Cheng, W.K., Hopkins, P.D., Komba, M., Carlow, D.A., Dutz, J.P., 2019. Topical Adjuvant Application during Subcutaneous Vaccination Promotes Resident Memory T Cell Generation. J. Immunol. 203, 2443–2450. https://doi.org/10.4049/jimmunol.1900199.
Li, Q.-Y., Zu, Y.-G., Shi, R.-Z., Yao, L.-P., 2006. Review Camptothecin: Current Perspectives. Curr. Med. Chem. 13, 2021–2039. https://doi.org/10.2174/092986706777585004.
Lin, J., Cai, Q., Tang, Y., Xu, Y., Wang, Q., Li, T., Xu, H., Wang, S., Fan, K., Liu, Z., Jin, Y., Lin, D., 2018. PEGylated Lipid bilayer coated mesoporous silica nanoparticles for co-delivery of paclitaxel and curcumin: Design, characterization and its cytotoxic effect. Int. J. Pharm. 536, 272–282. https://doi.org/10.1016/j.ijpharm.2017.10.043.
Llinàs, M.C., Martínez-Edo, G., Cascante, A., Porcar, I., Borrós, S., Sánchez-García, D., 2018. Preparation of a mesoporous silica-based nano-vehicle for dual DOX/CPT ph-triggered delivery. Drug Deliv. 25, 1137–1146. https://doi.org/10.1080/10717544.2018.1472678.
Lu, J., Liong, M., Zink, J.I., Tamanoi, F., 2007. Mesoporous silica nanoparticles as a delivery system for hydrophobic anticancer drugs. Small 3, 1341–1346. https://doi.org/10.1002/smll.200700005.
Min, J., Lip, Y., Han, S., Sung, D., Thambi, T., 2023. Injectable hydrogel imbibed with camptothecin-loaded mesoporous silica nanoparticles as an implantable sustained delivery depot for cancer therapy. J. Colloid Interface Sci. 636, 328–340. https://doi.org/10.1016/j.jcis.2023.01.028.
Momin, N., Palmeri, J.R., Lutz, E.A., Jailkhani, N., Mak, H., Tabet, A., Chinn, M.M., Kang, B.H., Spanoudaki, V., Hynes, R.O., Wittrup, K.D., 2022. Maximizing response to intratumoral immunotherapy in mice by tuning local retention. Nat. Commun. 13, 2041. https://doi.org/10.1038/s41467-021-27390-6.
Nhavene, E.P.F., Andrade, G.F., Arantes Faria, J.A.Q., Gomes, D.A., de Sousa, E.M.B., 2018. Biodegradable polymers grafted onto multifunctional mesoporous silica nanoparticles for gene delivery. ChemEngineering 2, 1–16. https://doi.org/10.3390/chemengineering2020024.
Oliveira, A.I., Pinho, C., Fonte, P., Sarmento, B., Dias, A.C.P., 2018. Development, characterization, antioxidant and hepatoprotective properties of poly(Ɛ-caprolactone) nanoparticles loaded with a neuroprotective fraction of Hypericum perforatum. Int. J. Biol. Macromol. 110, 185–196. https://doi.org/10.1016/j.ijbiomac.2017.10.103.
Otsuka, T., Nishida, S., Shibahara, T., Temizoz, B., Hamaguchi, M., Shiroyama, T., Kimura, K., Miyake, K., Hirata, H., Mizuno, Y., Yagita, M., Manabe, Y., Kuroda, E., Takeda, Y., Kida, H., Ishii, K.J., Kumanogoh, A., 2022. CpG ODN (K3)—toll-like receptor 9 agonist—induces Th1-type immune response and enhances cytotoxic activity in advanced lung cancer patients: a phase I study. BMC Cancer. 22, 744. https://doi.org/10.1186/s12885-022-09818-4.
Raina, N., Rani, R., Thakur, V.K., Gupta, M., 2023. New Insights in Topical Drug Delivery for Skin Disorders: From a Nanotechnological Perspective. ACS Omega. 8, 19145–19167. https://doi.org/10.1021/acsomega.2c08016.
Rev, P., Sharma, A., Chhikara, S., Ghodekar, S.N., Gawande, R., Namdeo, A.G., Mahadik, K.R., Fulzele, D.P., 2008. Review article camptothecin : discovery and developments. Phcog Rev. 2, 219–227 (doi not available).
Saini, K., Bandyopadhyaya, R., 2020. Transferrin-Conjugated Polymer-Coated Mesoporous Silica Nanoparticles Loaded with Gemcitabine for Killing Pancreatic

Cancer Cells. ACS Appl. Nano Mater. 3, 229–240. https://doi.org/10.1021/acsanm.9b01921.
Santoso, A.V., Susanto, A., Irawaty, W., Hadisoewignyo, L., Hartono, S.B., 2019. Chitosan modified mesoporous silica nanoparticles as a versatile drug carrier with pH dependent properties. AIP Conf. Proc. 2114 https://doi.org/10.1063/1.5112395.
Saroj, S., Rajput, S.J., 2018. Tailor-made pH-sensitive polyacrylic acid functionalized mesoporous silica nanoparticles for efficient and controlled delivery of anti-cancer drug Etoposide. Drug Dev. Ind. Pharm. 44, 1198–1211. https://doi.org/10.1080/03639045.2018.1438467.
Shah, P.V., Rajput, S.J., 2018. Facile Synthesis of Chitosan Capped Mesoporous Silica Nanoparticles: A pH Responsive Smart Delivery Platform for Raloxifene Hydrochloride. AAPS PharmSciTech 19, 1344–1357. https://doi.org/10.1208/s12249-017-0949-0.
Shakeran, Z., Keyhanfar, M., Varshosaz, J., Sutherland, D.S., 2021. Biodegradable nanocarriers based on chitosan-modified mesoporous silica nanoparticles for delivery of methotrexate for application in breast cancer treatment. Mater. Sci. Eng. C 118, 111526. https://doi.org/10.1016/j.msec.2020.111526.
Sharifi-Rad, J., Quispe, C., Butnariu, M., Rotariu, L.S., Sytar, O., Sestito, S., Rapposelli, S., Akram, M., Iqbal, M., Krishna, A., Kumar, N.V.A., Braga, S.S., Cardoso, S.M., Jafernik, K., Ekiert, H., Cruz-Martins, N., Szopa, A., Villagran, M., Mardones, L., Martorell, M., Docea, A.O., Calina, D., 2021. Chitosan nanoparticles as a promising tool in nanomedicine with particular emphasis on oncological treatment. Cancer Cell Int. 21, 1–21. https://doi.org/10.1186/s12935-021-02025-4.
Shehzad, A., Qureshi, M., Jabeen, S., Ahmad, R., Alabdalall, A.H., Aljafary, M.A., Al-Suhaimi, E., 2018. Synthesis, characterization and antibacterial activity of silver nanoparticles using Rhazya stricta. PeerJ. 2018, e6086.
Subramanian, N., Sundaraganesan, N., Sudha, S., Aroulmoji, V., Sockalingam, G.D., Bergamin, M., 2011. Experimental and theoretical investigation of the molecular and electronic structure of anticancer drug camptothecin. Spectrochim. Acta - Part A Mol. Biomol. Spectrosc. 78, 1058–1067. https://doi.org/10.1016/j.saa.2010.12.049.
Sun, X., Wang, N., Yang, L.Y., Ouyang, X.K., Huang, F., 2019. Folic acid and pei modified mesoporous silica for targeted delivery of curcumin. Pharmaceutics. 11, 430. https://doi.org/10.3390/pharmaceutics11090430.
Takahashi, M., Okamura, N., Ding, X., Shirakawa, H., Minamide, H., 2018. Intermolecular hydrogen bond stretching vibrations observed in terahertz spectra of crystalline vitamins. CrystEngComm. 20, 1960–1969. https://doi.org/10.1039/C8CE00095F.
Tao, C., Zhu, Y., Li, X., Hanagata, N., 2015. Binding of CpG oligodeoxynucleotides to mesoporous silica nanoparticles for enhancing delivery efficiency. Microporous Mesoporous Mater. 204, 91–98. https://doi.org/10.1016/j.micromeso.2014.11.007.
Vähätupa, M., Pemmari, T., Junttila, I., Pesu, M., Järvinen, T.A.H., 2019. Chemical-induced skin carcinogenesis model using dimethylbenz[a]anthracene and 12-o-tetradecanoyl phorbol-13-acetate (Dmba-tpa). J. vis. 154 https://doi.org/10.3791/60445.
Viegas, C., Pereira, D.S.M., Fonte, P., 2022. Insights into nanomedicine for head and neck cancer diagnosis and treatment. Materials (basel). 15, 2086. https://doi.org/10.3390/ma15062086.
Viegas, C., Patrício, A.B., Prata, J., Fonseca, L., Macedo, A.S., Duarte, S.O.D., Fonte, P., 2023. Advances in Pancreatic Cancer Treatment by Nano-Based Drug Delivery Systems. Pharmaceutics. 15, 2363. https://doi.org/10.3390/pharmaceutics15092363.
Viswanadh, M.K., Muthu, M.S., 2018. Targeted bioadhesive nanomedicine: An effective approach for synergistic drug delivery to cancers. Nanomedicine 13, 1401–1403. https://doi.org/10.2217/nnm-2018-0114.
Voiculescu, V.M., Lisievici, C.V., Lupu, M., Vajaitu, C., Draghici, C.C., Popa, A.V., Solomon, I., Sebe, T.I., Constantin, M.M., Caruntu, C., 2019. Mediators of inflammation in topical therapy of skin cancers. Mediators Inflamm. 2019, 8369690. https://doi.org/10.1155/2019/8369690.
Wang, N., Cheng, X., Li, N., Wang, H., Chen, H., 2019. Nanocarriers and their loading strategies. Adv. Healthc. Mater. 8, 1–26. https://doi.org/10.1002/adhm.201801002.
Werner stober, A.F., 1968. Controlled Growth of Monodisperse Silica Spheres in the Micron Size Range 1 werner. J. Colloid Interface Sci. 26, 62–69. https://doi.org/10.1016/0021-9797(68)90272-5.
Xu, Y., Claiden, P., Zhu, Y., Morita, H., Hanagata, N., 2015. Effect of amino groups of mesoporous silica nanoparticles on CpG oligodexynucleotide delivery. Sci. Technol. Adv. Mater. 16, 045006 https://doi.org/10.1088/1468-6996/16/4/045006.
Yan, L., Shen, J., Wang, J., Yang, X., Dong, S., Lu, S., 2020. Nanoparticle-Based Drug Delivery System: A Patient-Friendly Chemotherapy for Oncology. Dose-Response 18, 1–12. https://doi.org/10.1177/1559325820936161.
Yu, L., Luo, Z., Chen, T., Ouyang, Y., Xiao, L., Liang, S., Peng, Z., Liu, Y., Deng, Y., 2022. Bioadhesive Nanoparticles for Local Drug Delivery. Int. J. Mol. Sci. 23, 2370. https://doi.org/10.3390/ijms23042370.
Zaharudin, N.S., Mohamed Isa, E.D., Ahmad, H., Abdul Rahman, M.B., Jumbri, K., 2020. Functionalized mesoporous silica nanoparticles templated by pyridinium ionic liquid for hydrophilic and hydrophobic drug release application. J. Saudi Chem. Soc. 24, 289–302. https://doi.org/10.1016/j.jscs.2020.01.003.
Zhang, H., Lai, L., Wang, Y., Ye, B., Deng, S., Ding, A., Teng, L., Qiu, L., Chen, J., 2019. Controlled Release and Delivery Systems Silk fibroin for CpG oligodeoxynucleotides delivery. Pharmaceutics. 11, 494. https://doi.org/10.1021/acsbiomaterials.9b01413.
Zhang, X., Lin, Y., Gillies, R.J., 2010. Tumor pH and its measurement. J. Nucl. Med. 51, 1167–1170. https://doi.org/10.2967/jnumed.109.068981.
Zhou, Y., Quan, G., Wu, Q., Zhang, X., Niu, B., Wu, B., Huang, Y., Pan, X., Wu, C., 2018. Mesoporous silica nanoparticles for drug and gene delivery. Acta Pharm. Sin. B 8, 165–177. https://doi.org/10.1016/j.apsb.2018.01.007.